VOID FORMATION AND COLLAPSE IN NANOWIRES

O.M. PODOLYAN, T.V. ZAPOROZHETS

B. Khmelnytskyi Cherkasy National University
(81, Shevchenko Blvd., Cherkasy, Ukraine; e-mail: ompodolyan@mail.ru)

PACS 61.46.c; 61.46.p; 61.72.jd; 64.75.Nx; 64.76.Op; 66.10.C

The two-stage process of formation and collapse of hollow nanowires in core-shell systems is described in the framework of the phenomenological model of solid solutions as a result of the competition of the Frenkel effect, Gibbs–Thomson effect, and inverse Kirkendall effect. The dependences of the pore formation rate and efficiency on the initial cylinder radius and the fast component concentration are studied. The obtained results are compared with similar ones known for spherically symmetric particles. It is shown that the pore formation is more effective in cylindrical samples as compared to spherical ones, whereas the existence time of a void depends on the nanoshell radius.

1. Introduction

Pore formation in core-shell systems was first registered in spherically symmetric microparticles of Be/Ni [1] and Cd/Ni[2, 3] systems. Thirty years later, this phenomenon was rediscovered in spherical Co/Se [4], Co/O [4], Co/S [4, 5], Fe/O [6], Al/O [7], Cu/O [7, 8], Zn/O [9], and Ni/O [10] nanosystems, as well as in ZnO/Al_2O_3 [11] and Fe/O [12] systems with cylindrical symmetry. The production of such particles has immediately found a wide application in many scientific and technological researches (starting from the fabrication of porous nanomaterials and finishing with the Drug Delivery technology in medicine [13]). However, the obtained hollow nanoshells can be extremely widely used only if being stable or metastable under certain conditions. It was theoretically predicted [14, 15] and experimentally confirmed [16] that the collapse of a nanoshell is always energy-profitable, as it leads to a decrease of the surface energy. Metastable voids can be obtained by changing external conditions. For example, it is sufficient that the operation temperature of hollow nanoparticles be by 100–200 K lower than the temperature of their formation, because the shrinking time is inversely proportional to the diffusion coefficient [15]. And *vice versa*, an increase of the temperature results in a faster void collapse. For example, nanoshells obtained within an hour at 373 K due to the oxidation of copper nanoparticles with a mean diameter of 30 nm remain metastable at this temperature [7], whereas the collapse of such voids during the same time interval is possible only at 523 K [16]. As far as we know, there are no experimental studies for metal/nonmetal systems, in which the formation and the collapse of nanovoids are considered as two stages of a single process under constant external conditions (temperature and pressure). Recently, however, the phenomenological estimates and the computer simulation of a spherically symmetric diffusion pair of metals performed on the atomic level in [17] allowed one to choose such a pair and investigate the void formation and collapse in a single continuous experiment for the semispherical "Ag core/Au shell" system [18].

Work [17] proposes phenomenological and simulation models of the formation and the collapse of a nanoshell as two stages of a single process for spherical nanoparticles of a binary system with complete solubility or, at least, a wide homogeneity interval. In this study, we investigate a system with cylindrical symmetry. We are aimed at the creation of a phenomenological model of pore formation in cylindrically symmetric nanoparticles, i.e. nanowires, as well as the derivation of quantitative estimates with fitting parameters for nanospheres [17] and the comparison of the obtained estimates with the corresponding results derived for spherical nanoshells [17]. In the authors' opinion, fitting parameters do not decrease the value of the comparative analysis that can

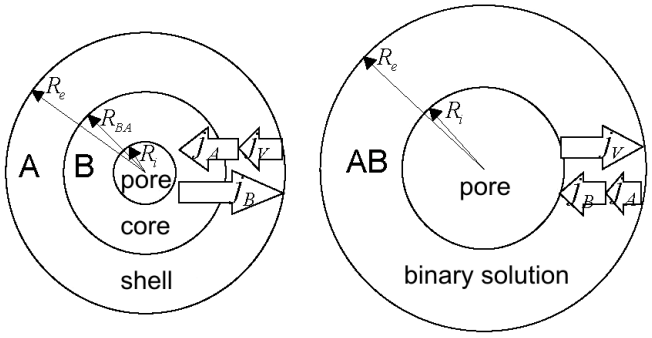

Fig. 1. Diagram of void formation (a) and collapse (b) in the cylindrical system "core B/shell A" with radial symmetry and the radius of the fast-component core R_{BA}. At the formation stage, the vacancy flux j_V is directed inside opposite to the flux of the fast component j_B and compensates the flux of the slow component j_A. At the collapse stage, the vacancy flux j_V is directed from the inner surface R_i with a higher vacancy concentration to the outer one R_e (with a lower vacancy concentration). Moreover, the vacancy flux induces opposite fluxes of components A and B.

be useful for subsequent experiments, which is proved by studies [16, 18] referring to the corresponding theoretical predictions [15, 17].

In his pioneer work [1], Aldinger explained the origination of pores by the fast diffusion of core atoms (Be) to the shell of the surrounding element (Ni) with much smaller diffusion mobility. The described phenomenon is characteristic of the reaction diffusion in binary systems with closed geometry restricting the lattice motion. The main reason for the pore formation is the difference between the partial diffusion coefficients of the components resulting in the difference of the atom fluxes j_A and j_B in the lattice system (Fig. 1, a, B is the fast component and A is the slow one). To compensate this difference, there arises a vacancy flux j_V directed toward the faster component. In this case, a radial redistribution of vacancies (with an initial maximum at the contact zone) takes place: the region of the fast component is enriched with vacancies, while that of the slow one is depleted. If the vacancy sinks are not very effective, then nonequilibrium vacancies in the fast-component region must accumulate into pores (Frenkel effect). Surely, such an accumulation can be possible and noticeable on a curved surface, if the fast component is surrounded by the slow one, for example, in spherical or cylindrical samples that form a core-shell system. In [4–9, 11, 12, 16, 19], the pore formation is considered as a result of the reaction diffusion of metal particles with oxygen/sulfur: the diffusion of a metal "outside" through the newly formed spherical interlayer takes place faster than the diffusion of oxygen or sulfur "inside" through the same region; the difference of these fluxes gives rise to a vacancy flux inside the nanoparticle that leads to the vacancy supersaturation and the pore formation. In the foreign literature (and particularly in [4]), the Frenkel effect is called the Kirkendall pore formation, which results in an ambiguity [19], because Kirkendall shifts and Kirkendall pores represent different and, what is more, competing effects caused by the same reason (different partial diffusion coefficients).

The instability of hollow nanoparticles caused by the excess surface energy leads to a collapse provided by the Gibbs–Thomson effect: the vacancy concentration on the outer surface (with a larger radius of curvature R_e) is smaller than on the inner one (with a lower radius of curvature R_i and different sign). This difference in the concentrations induces a vacancy flux coming outside and results in the nanoshell collapse (Fig. 1, b). In the case of a binary shell, the difference in the mobilities of the components will result in the segregation of the faster component in a vicinity of the inner surface (inverse Kirkendall effect), which will decelerate, in turn, the vacancy flux. That is why a conclusion can be made that the collapse is controlled by the slower component [15, 16].

As was shown in [20], it is important to take the Gibbs-Thomson effect into account already on the stage of nanovoid formation: the formation of a strongly curved inner surface immediately induces an inverse vacancy flux that impedes the vacancy flux coming from outside. Sometimes, it even can exceed the latter, completely suppress the growth of a void, and result in its collapse. That is why it is important to allow for the evolution of the concentration distributions and the Laplace pressure both on the collapse and formation stages.

Thus, on the stage of void formation in an immobile lattice system, the Frenkel effect, arising due to the gradient of the chemical potential in the diffusion pair, competes with the Gibbs–Thomson effect; on the collapse stage, the Gibbs–Thomson effect competes with the inverse Kirkendall effect.

2. Phenomenological Model

First, let us consider the collapse of a hollow nanotube of a binary solid solution with a wide homogeneity interval. To describe the void formation in a two-component nanowire with the cylinder-shell geometry, it is enough to change the initial conditions in the collapse model similarly to the description of spherical nanoshells [13]. In this case, the main assumption of the model is the formation of an initially cylindrically symmetric pore along the whole axis of the nanowire, i.e. the formation of a

hollow nanotube (the validity of this assumption is discussed in what follows).

2.1. Collapse of a hollow nanowire

We consider a hollow nanotube, whose atomic structure corresponds to a binary solid solution with a wide homogeneity interval. Let us first discuss the collapse stage of a centrally symmetric void in the nanotube. To describe the formation stage, it is necessary to take into account the vacancy flux induced by the difference of the vacancy concentrations at the inner and outer boundaries. In the case of solid solution, the diffusion coefficients and concentrations cannot be considered constant quantities, so one should solve a system of nonlinear equations for the vacancy fluxes, basic components, and boundary motion.

2.1.1. Model approximation

1. The diffusion coefficients of the both components are proportional to the local vacancy concentration c_V:

$$D_A^*\left(c_B\right) = c_V K_A\left(c_B\right), D_B^*\left(c_B\right) = c_V K_B\left(c_B\right), \tag{1}$$

while the proportionality coefficients, in turn, exponentially depend on the concentration of the components, which is a typical situation [21]:

$$K_A\left(c_B\right) = K_{A0}\exp\left(\alpha_A c_B\right),$$

$$K_B\left(c_B\right) = K_{B0}\exp\left(\alpha_B c_B\right), \tag{2}$$

where c_B is the molar portion of component B.

2. Diffusion fluxes of the basic components and vacancies take crossed terms into account. In the lattice reference system, they can be written down as [2, 22]

$$\Omega j_A\left(r\right) = -D_A^*\varphi\frac{\partial c_A}{\partial r} + \frac{c_A D_A^*}{c_V}\frac{\partial c_V}{\partial r} =$$

$$= +K_A\varphi c_V\frac{\partial c_B}{\partial r} + c_A K_A\frac{\partial c_V}{\partial r}, \tag{3}$$

$$\Omega j_B\left(r\right) = -D_B^*\varphi\frac{\partial c_B}{\partial r} + \frac{c_B D_B^*}{c_V}\frac{\partial c_V}{\partial r} =$$

$$= -K_B\varphi c_V\frac{\partial c_B}{\partial r} + c_B K_B\frac{\partial c_V}{\partial r}, \tag{4}$$

$$\Omega j_V\left(r\right) = \left(K_B - K_A\right)\varphi c_V\frac{\partial c_B}{\partial r} -$$

$$-\left(c_A K_A + c_B K_B\right)\frac{\partial c_V}{\partial r}, \tag{5}$$

where the thermodynamic factor $\varphi = \frac{c_A c_B}{kT}\frac{\partial^2 g}{\partial c_B^2}$, g is the free Gibbs energy per solid-solution atom, and Ω is the atomic volume.

3. In the absence of the Kirkendall effect, the boundaries move due to transitions of atoms from one surface to another rather than due to a shift of the lattice. This assumption results in the balance equation (similarly to the second Fick law) in the lattice reference system:

$$\frac{\partial c_V}{\partial t} = -\frac{1}{r}\frac{\partial}{\partial r}\left(r\Omega j_V\right) + 0, \tag{6}$$

$$\frac{\partial c_B}{\partial t} = -\frac{1}{r}\frac{\partial}{\partial r}\left(r\Omega j_B\right). \tag{7}$$

Zero in Eq. (6) indicates the absence of vacancy sinks and sources inside the nanocylinder.

2.1.2. Boundary conditions

The vacancy distribution $c_V\left(r,t\right)$ is nonequilibrium in both the processes of collapse and formation. But its values at the boundaries (inner and outer surfaces) are equilibrium and determined by the Gibbs-Thomson equations

$$c_V\left(R_i\right) = c_V^{\mathrm{eq}}\exp\left(+\frac{\gamma\Omega}{kT}\frac{1}{R_i}\right),$$

$$c_V\left(R_e\right) = c_V^{\mathrm{eq}}\exp\left(-\frac{\gamma\Omega}{kT}\frac{1}{R_e}\right), \tag{8}$$

where c_V^{eq} is the equilibrium vacancy concentration in a vicinity of the plane surface, γ stands for the surface tension, k is the Boltzmann constant, T is the temperature, while R_i and R_e are the inner and outer radii of the shell, respectively.

The balance equations for the fluxes at the inner and outer moving boundaries depend on the experimental conditions. We consider the case where there is no evaporation of atoms from the nanoshell, so all fluxes outside the shell and inside the pore are absent. The vacancy flux from the inner boundary to the outer one results in the motion of these boundaries according to the equations

$$\frac{dR_i}{dt} = -\Omega j_V\left(R_i\right), \frac{dR_e}{dt} = -\Omega j_V\left(R_e\right). \tag{9}$$

The boundary conditions (8) and (9) are sufficient in the case of the collapse of a one-component shell. If considering a binary solution, it is necessary to introduce additional conditions. As the boundary concentrations of the basic components are not fixed (there is no analog of Eq. (8) for components A or B), though the conservation laws are fulfilled, the sum of the fluxes in the lattice reference system equals zero: $j_V + j_A + j_B = 0$. Thus, only two fluxes are independent. That is why the use of the balance equation for the fluxes at the inner and outer moving boundaries for one of the basic components provides the condition that the fluxes outside the shell are zero. We obtain, respectively,

$$-c_B(R_i)\,\Omega j_V = \Omega j_B(R_i),$$

$$-c_B(R_e)\,\Omega j_V = \Omega j_B(R_e). \tag{10}$$

After that, the vacancy diffusion is described with the use of a common stationary approximation that reflects the hierarchy of characteristic times – the vacancy subsystem adopts rather fast to the slow redistribution of the basic components and the motion of the boundaries (except for the last collapse stage that is very rapid):

$$\frac{\partial c_V}{\partial t} \approx 0 \quad \Rightarrow \quad r\Omega j_V(r) = \frac{\Omega J_V}{2\pi H} = \text{const} \quad \text{for } r \tag{11}$$

(J_V is the total vacancy flux determined from the boundary conditions, and H is the cylinder length).

To simplify the further mathematical transformations, it is convenient to use new variables

$$t' = t; \xi = \frac{\ln R_e - \ln r}{\ln R_e - \ln R_i}, 0 < \xi < 1, \tag{12}$$

$$\frac{\partial}{\partial t} = \frac{\partial}{\partial t'} + \frac{\xi \frac{1}{R_i}\frac{dR_i}{dt} + (1-\xi)\frac{1}{R_e}\frac{dR_e}{dt}}{\ln \frac{R_e}{R_i}} \frac{\partial}{\partial \xi},$$

$$r\frac{\partial}{\partial r} = -\frac{1}{\ln \frac{R_e}{R_i}} \frac{\partial}{\partial \xi}. \tag{13}$$

Using Eqs. (11, 5, 12, and 13), we obtain

$$\frac{\partial c_V}{\partial \xi} = \frac{(K_B - K_A)\,\phi c_V}{c_A K_A + c_B K_B} \frac{\partial c_B}{\partial \xi} + \frac{\ln \frac{R_e}{R_i}}{c_A K_A + c_B K_B} \frac{\Omega J_V}{2\pi H}. \tag{14}$$

If the profile $c_B(\xi)$ is known, then Eq.(13) will have the standard form

$$\frac{dc_V(\xi)}{d\xi} = f(\xi)\, c_V + \frac{\text{const}}{\psi(\xi)}, \tag{15}$$

where

$$\psi(\xi) = c_A(\xi) K_A(\xi) + c_B(\xi) K_B(\xi),$$

$$f(\xi) = \frac{(K_B - K_A)\,\varphi}{c_A K_A + c_B K_B} \frac{\partial c_B}{\partial \xi}, \quad \text{const} = \frac{\Omega J_V}{2\pi H} \ln \frac{R_e}{R_i}, \tag{16}$$

and can be solved for the unknown function $c_V(\xi)$:

$$c_V(\xi) = \exp\left(\int_0^{\xi} f(\xi')d\xi'\right)\left(c_V^{\text{eq}} \exp\left(-\frac{\gamma\Omega}{kTR_e}\right) + \right.$$

$$\left. + \ln \frac{R_e}{R_i} \frac{\Omega J_V}{2\pi H} \int_0^{\xi} \frac{d\xi'}{\psi(\xi')} \exp\left(-\int_0^{\xi'} f(\xi'')\, d\xi''\right)\right). \tag{17}$$

Combining expression (17) with the Gibbs–Thomson equation (8) for the boundary vacancy concentrations, we obtain the expression for the total vacancy flux through the unknown concentration profile of component B:

$$\frac{\Omega J_V}{2\pi H} = \frac{1}{\ln \frac{R_e}{R_i}} \times$$

$$\times c_V^{\text{eq}} \frac{\exp\left(\frac{\gamma\Omega}{kTR_i}\right) \exp\left(-\int_0^1 f(\xi)\, d\xi\right) - \exp\left(-\frac{\gamma\Omega}{kTR_e}\right)}{\int_0^1 \exp\left(-\int_0^{\xi} f(\xi')\, d\xi'\right) \frac{d\xi}{\psi(\xi)}}. \tag{18}$$

Substituting Eq. (13) into Eq. (4), the flux of one of the basic components can be expressed in terms of its gradient and the total vacancy flux (that is constant within the interlayer $\partial\xi$):

$$r\Omega j_B(r) = -K_B \phi c_V r \frac{\partial c_B}{\partial r} + c_B K_B r \frac{\partial c_V}{\partial r} =$$

$$= \frac{1}{\ln \frac{R_e}{R_i}} \frac{K_A K_B \phi c_V}{c_A K_A + c_B K_B} \frac{\partial c_B}{\partial \xi} - \frac{c_B K_B}{c_A K_A + c_B K_B} \frac{\Omega J_V}{2\pi H}. \tag{19}$$

Thus, the stationary approximation for vacancies together with the Gibbs–Thomson boundary conditions reduce the system of two differential equations (4) and (7)

with regard for (14) to one, though integro-differential, equation:

$$\frac{\partial c_B}{\partial t'} = -\frac{\xi \frac{1}{R_i}\frac{dR_i}{dt} + (1-\xi)\frac{1}{R_e}\frac{dR_e}{dt}}{\ln\frac{R_e}{R_i}}\frac{\partial c_B}{\partial \xi} +$$

$$+\frac{1}{R_i^{2\xi}R_e^{2(1-\xi)}}\frac{1}{\ln\frac{R_e}{R_i}}\frac{\partial}{\partial\xi}\left(\frac{1}{\ln\frac{R_e}{R_i}}\frac{K_A K_B \phi(\xi)}{c_A K_A + c_B K_B}\times\right.$$

$$\left.\times c_V(\xi)\frac{\partial c_B}{\partial \xi} - \frac{c_B K_B}{c_A K_A + c_B K_B}\frac{\Omega J_V}{2\pi H}\right). \quad (20)$$

The total vacancy flux in Eq. (20) is determined by Eq. (18). The boundary conditions for the profile of component B at the inner ($\xi = 1$) and outer ($\xi = 0$) boundaries are determined from Eq. (10) with regard for Eqs. (18 and 19):

$$\left.\frac{\partial c_B}{\partial \xi}\right|_{\xi=1} = \ln\frac{R_e}{R_i}\frac{\Omega J_V}{2\pi L}\frac{c_A c_B (K_B - K_A)}{K_A K_B \varphi}\times$$

$$\times\exp\left(-\frac{\gamma\Omega}{kTR_i}\right)\Big/ c_V^{\rm eq}, \quad (21)$$

$$\left.\frac{\partial c_B}{\partial \xi}\right|_{\xi=0} = \ln\frac{R_e}{R_i}\frac{\Omega J_V}{2\pi L}\frac{c_A c_B (K_B - K_A)}{K_A K_B \varphi}\times$$

$$\times\exp\left(\frac{\gamma\Omega}{kTR_e}\right)\Big/ c_V^{\rm eq}. \quad (22)$$

2.1.3. Algorithm of the numerical iteration procedure

The boundary-value problem (20)–(22) is solved with the help of an explicit finite-difference scheme. The profile of component B at the previous time step is used to calculate the total vacancy flux (18) substituted into Eq. (20) to find the profile at the next time step. After that, the newly calculated profile of component B and the total vacancy flux are used to derive the new vacancy profile according to Eq. (17) with boundary conditions (8). The velocities of the boundaries (new inner and outer radii) are calculated at each iteration step according to Eq. (9) based on the just found value of the total vacancy flux (18).

The choice of a time step in the iteration scheme represents a rather complicated problem in the simulation of the described process: there is a risk of obtaining the invalid time evolution of the system, at which the scheme remains stable and, at first sight, yields a qualitatively correct result, though leads to a significant error of the finite-difference method and the non-conservation of the mean concentration of the diffusion pair. In addition, a slight variation of the radial dimensions of the system results in the power change of the time scales of the process (which will be confirmed in what follows by the simulation results (see Fig. 8). So, to obtain a reachable simulation time, the time steps should be chosen individually (their difference for small and large samples reached five orders of magnitude, $dt = 10^{-5} \div 1$s).

The instability of the scheme is caused by the mobile boundaries (9) and the non-uniform scale (12). The use of the non-uniform coordinate scale results in a low density of the points of the concentration profiles in a vicinity of the outer surface. This fact should be taken into account in the case of the increase of the particle radius and especially increase of the concentration of the inner component if the outer one occupies a very narrow interlayer (with regard for the power dependence of the volume on the radius).

That is why each calculation with fixed concentration and outer particle radius was performed, by choosing such a number of points of the concentration profiles to provide the deviation of the average concentration at each time moment within 1%. According to the space discretization and with regard for the pore formation rate, we chose a variable time step in the iteration procedure. The best criterion of stability of the scheme was the gradient of the average concentration that must not exceed 10^{-3} s^{-1} for cylinders and 10^{-4} s^{-1} for spheres. The technical realization of this criterion was performed using the predictor-corrector scheme.

2.2. Formation of a hollow nanocylinder in the core-shell system

To describe the stage of pore formation in a nanowire, it is enough to change only initial conditions in the above-proposed model. The only necessary condition of its applicability is the presence (from the very beginning) of a small cylindrical void along the cylinder axis. Here, it is worth noting two warnings with the corresponding substantiation.

First, in a system with large initial core radius, one actually observes the simultaneous origination of many voids at the inner interface of the newly formed solid-solution interlayer ("bridge model" [5, 6, 11]). That is why our model can be applied only to studying small particles characterized by the fast coalescence of initial

voids and the optimization of the surface energy, which results in the formation of one central cylindrical void. The applicability limits of the model can be estimated, by finding the vacancy supersaturation and the critical void volume at the origination that determine the size of the spherical region, from which vacancies are collected at this time moment. If the radius of the supersaturation region, from which vacancies are "collected", is close to R_{BA} (but does not exceed it!), the only pore will be formed along the cylinder axis; if it will be much lower, the formation of several pores will be observed. It is a subject of a separate study that must be performed by means of a Monte Carlo simulation on the atomic level.

Second, for a system with a small radius of the fast-component initial core or a small thermodynamic stimulus, the critical pore radius determined by the competition of the Frenkel and Gibbs–Thomson effects can appear lower than the radius R_{i0} of the initiated pore [20]. As a result, the system will immediately appear at the collapse stage, and the model will operate consistently.

To study the formation stage, it is necessary to decrease the initial pore size together with the time step in the finite-difference scheme in order to provide its valid operation — the process will run much faster for a more curved trajectory. The collapse at non-physically small radii of the initial pore (of the order of the interatomic distance) should be understood as the impossibility of the pore formation in principle.

Thus, the phenomenological simulation of the formation process considers a cylindrical core-shell system with the core radius (pure component B) R_{BA}, shell radius (pure component A) $R_e = R_{e0}$, and the radius of the initial pore $R_i = R_{i0}$ (of the order of the lattice constant). The initial profile of component B is specified as:

$$t' = 0, c_B(\xi) = \begin{cases} 1, & 0 < \xi < \xi_{BA}, \\ 0, & \xi_{BA} < \xi < 1, \end{cases}$$

$$\xi_{BA} \equiv \frac{\ln R_{e0} - \ln R_{BA}}{\ln R_{e0} - \ln R_{i0}}. \tag{23}$$

3. Results and Discussion

For the qualitative investigation of the constructed phenomenological model of formation/collapse of hollow nanotubes and the comparison of the results with those obtained using a similar model for hollow nanospheres, we used the parameters given in [17]: $c_v^{\mathrm{eq}} = 10^{-4}$, $\gamma\Omega/kT = 0.375$ nm, $K_{A0} = 10^{-16}$ m^2/s, $K_{B0} = 10^{-15}$ m^2/s, $\alpha_A = -4.5$, $\alpha_B = -2$, and $\phi = 1$.

The choice of the parameters is somewhat conditional, but the basic qualitative results do not depend on specific parameters. Particularly, a decrease of the equilibrium vacancy concentration by a factor of n is equivalent to the renormalization of the time scale (i.e. the characteristic times of formation/collapse of a nanovoid will increase by a factor of n, as c_v^{eq} linearly enters all equations). An increase of the characteristic length in the Gibbs–Thomson effect $\gamma\Omega/kT$ will rise the role of capillary phenomena in the competition of the effects that determine the void formation and collapse. It is also worth noting that, according to estimates obtained from simulations by the molecular dynamics and molecular statics methods [23, 24], one should expect that the vacancy concentration in vicinities of the inner and outer boundaries of a nanoshell considerably exceeds the equilibrium concentration in a macrocrystal. That is why the average vacancy concentration in a nanoshell can significantly exceed tabular values.

The average concentration of the fast component $\overline{c}_B$ was varied (0.075, 0.1, 0.2, 0.3, 0.4, 0.5, 0.6, 0.7, 0.8, 0.9, 0.925) and determined the radius R_{BA} of the B/A interface (Fig. 1,*a*). Such an investigation of the pore formation in the wide range of concentrations can be useful, because the average concentration can be used as a regulating parameter for obtaining the desirable sizes of voids and the times of their existence. The case with a low concentration of the fast component can be realized under oxidation/ sulfidation [4, 5, 7–12], at which the matrix of the slow component can be considered as a source with infinite power.

The initial outer radius R_{e0} that determines the radius of an initial nanowire was logarithmically changed from $3a$ to $34a$ (this range of values covers the characteristic sizes of nanoparticles given in experimental works).

The proposed model does not consider the nucleation stage. To provide the consistent operation of the numerical phenomenological scheme, we specify, instead of, an initial pore of non-zero radius $R_{i0} = a$ (a is the lattice constant of the metal of the order of several angströms). In a restricted open nanosystem, the moving force (supersaturation) changes with time, that is why the description of the nucleation stage represents a separate problem that will be thoroughly analyzed in another work. The assumption about the existence of an initial pore can be considered valid under the condition that the characteristic time of growth of the pore is much larger than the time of its origination. That is why we make the simplest estimates on the basis of the empirical rules from the pore formation thermodynamics. Namely, there is a generally accepted empirical rule in the physics

of materials, according to which the nucleation is possible during a real time interval only if the height of the pore formation barrier ΔG^* is smaller than $60kT$ [25] (in some sources, $70kT$ [26]). The nucleation time of a new phase is of the order of seconds if the barrier is $30kT - 40kT$ [27]. If it decreases to kT, then the nucleation takes place immediately (as a result of the first thermal fluctuation). In our estimates, we neglect the peculiarities of pore formation in the nanosystem. Both the critical radius r_{cr} and the barrier height ΔG^* change in time:

$$r_{cr}(t) = \frac{2\gamma\Omega}{kT\ln\left(c_V(t)/c_V^{\rm eq}\right)}, \Delta G^*(t) = 1/3\gamma 4\pi r_{cr}^2. \quad (24)$$

It is caused by the increase in the concentration of vacancies accumulated during the process of mutual diffusion due to the difference between the partial diffusion coefficients:

$$c_V(t) \approx c_V^{\rm eq} + \frac{2}{R_{BA}}\int\limits_0^t \Omega j_V(R_{BA}, t')\,dt'. \quad (25)$$

If $D_B \gg D_A$, then

$$\Omega j_V \approx -\Omega j_B \approx \sqrt{\frac{D_B}{\pi t}}. \quad (26)$$

The substitution of (26) into (25) yields

$$c_V(t) \approx c_V^{\rm eq} + \frac{4}{R_{BA}}\sqrt{\frac{D_B}{\pi t}}. \quad (27)$$

Let us introduce a reduced nucleation barrier $\mathrm{E} = \Delta G^*/kT$. Combining formulas (24)–(27), we obtain that the pore formation barrier decreases to the specified value E during the time

$$t(\mathrm{E}) \approx \frac{\left(c_V^{\rm eq}R_{BA}\right)^2}{16D_B}\left(\exp\left(\frac{2\pi}{3\mathrm{E}}\frac{1}{\Omega}\left(\frac{2\gamma\Omega}{kT}\right)^3\right) - 1\right). \quad (28)$$

A pore will inevitably originate within the time interval $[t(60), t(1)]$, during which the barrier height ΔG^* appears in the range $[60kT, kT]$. At the used parameters, the upper limit of the time interval is by several orders of magnitude smaller than the characteristic time of growth of the pore at the corresponding radii $R_{BA} = \sqrt[3]{\bar{c}_B\left(R_{e0}^3 - R_{i0}^3\right) + R_{i0}^3}$ (Fig. 8). Thus, the neglect of the nucleation stage is valid in this problem.

The time evolution obtained as a result of the phenomenological simulation of the formation and the collapse of a hollow nanocylinder considered as two successive stages of the single pore formation process under invariable external conditions (Fig. 2) qualitatively

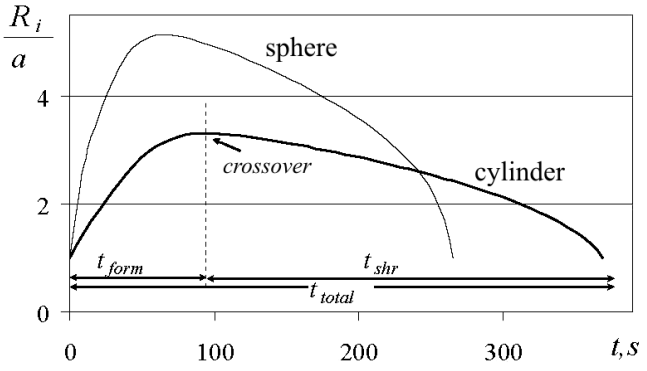

Fig. 2. Time evolution of a pore in a cylinder and a sphere [17] – the fast formation stage $t_{\rm form}$ is followed by the slower collapse stage $t_{\rm shr}$. $R_{e0} = 15.2a$, $\bar{c}_B = 0.075$

agrees with the similar results obtained for nanospheres [17]. The crossover point corresponds to the moment of transition from one stage to another. The stages are respectively characterized by the formation time $t_{\rm form}$ and the shrinking time $t_{\rm shr}$, whose relation determines the relative stability of the pore.

The radius of the maximal pore $R_i^{\max}$ reached at the crossover moment (Fig. 2) at the average concentration $\bar{c}_B = 0.075$ depends almost linearly on the initial particle radius R_{e0} both for spherical and for cylindrical samples (Fig. 3). The deviation from the linear law at small initial radii is explained by the existence of the initial centrally symmetric pore along the cylinder axis with the radius a, which is a necessary condition for consistent calculations in the given phenomenological model. It is evident that, for small real core-shell systems with the prevalence of one of the components, the chemical moving forces can appear insufficient for the formation (or even for nucleation [20]) of a pore with an effective radius exceeding a. In other words, the artificial introduction of an initial pore "makes" the system forming a void with a radius not less than a.

An increase of the average concentration of the fast component $\bar{c}_B$ does not result in a change of the linear character of the dependence $R_i^{\max}(R_{e0})$ (Fig. 4). In the case of large concentrations and small radii, however, the linear law is again violated. It is caused by a reduction of the reserve of chemical moving forces in the same way as at low concentrations. Moreover, the situation worsens due to the non-symmetry of the mobilities of the components (the faster internal component B cannot dissolve in shell A and the radial vacancy flux coming inside the cylinder is very small). If introducing a restriction on cylinders with small radii at the corresponding average concentrations $R_{e0}^{\min}$ (Table), then the error of the linear

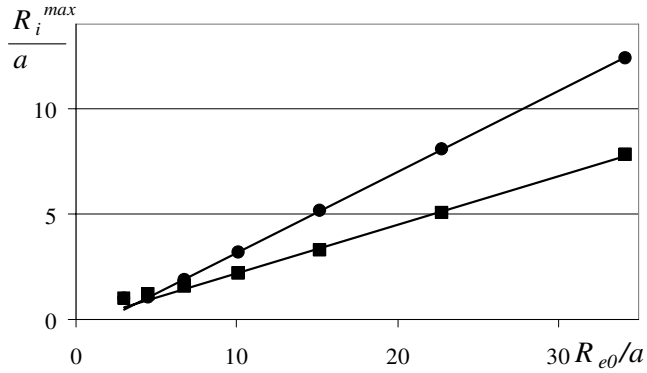

Fig. 3. Maximum pore radius $R_i^{\max}$ as a function of the initial radius of the particle R_{e0} for spheres (circles) and cylinders (squares). $\bar{c}_B = 0.075$

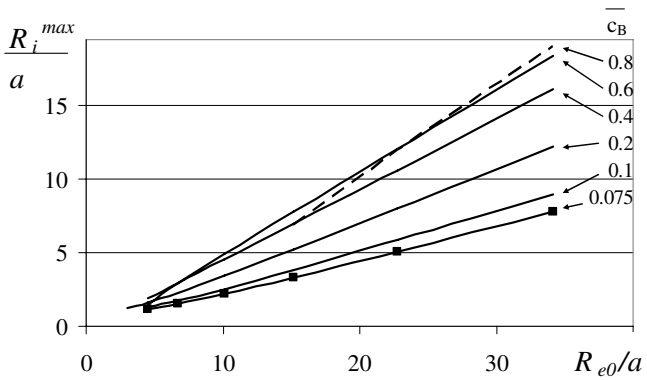

Fig. 4. Maximum pore radius $R_i^{\max}$ as a function of the initial radius of the particle R_{e0} for cylinders at various average concentrations $\bar{c}_B$

approximation $R_i^{\max} \sim k(\bar{c}_B) R_{e0} + b(\bar{c}_B)$ at a fixed average concentration will not exceed 0.2%. To realize a correct approximation at $\bar{c}_B > 0.8$, one should consider cylinders with $R_{e0} > 34a$, that is why the Table contains data for $\bar{c}_B \leq 0.8$.

For the specified diffusion parameters of the model, the slope $k(\bar{c}_B)$ of the approximation straight lines $R_i^{\max}(R_{e0})$ in the interval $0 < \bar{c}_B \leq 0.8$ is proportional to the square root of the average concentration of the fast component: $k(\bar{c}_B) \sim 0.75\sqrt{\bar{c}_B}$ (Table). The obtained approximate dependence demonstrates that a pore can occupy nearly a half of the initial volume of the fast component with the initial radius R_{BA}: $\pi (R_i^{\max})^2 H \sim \pi 0.56 \bar{c}_B (R_{e0})^2 H \sim 0.56\pi (R_{BA})^2 H$. This relation yields understated values of the maximal pore radius $R_i^{\max}$ at low concentrations (small amount of the mobile component very rapidly dissolves in the matrix of the slow one). At high concentrations, these values are overestimated (chemical moving forces come

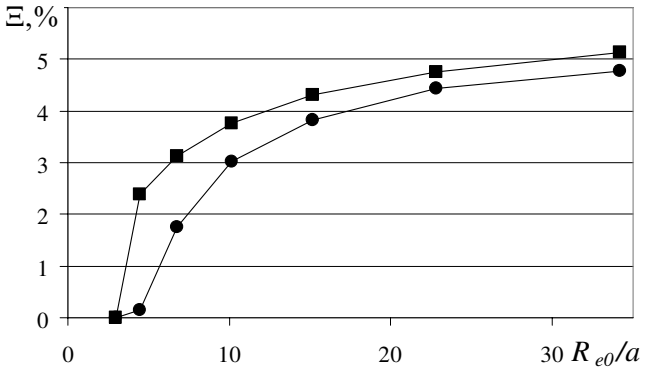

Fig. 5. Pore formation efficiency Ξ as a function of the initial radius of the particle R_{e0} for spheres (circles) and cylinders (squares). $\bar{c}_B = 0.075$

to the end much faster than the diffusion homogenization takes place; at some sets of parameters, a thick interlayer of pure component B, which had no time to react, is still observed on the inner surface after the crossover is already reached). The indicated deviations are corrected by taking the linear approximation coefficient b into account (see Table).

To analyze the pore formation efficiency, let us consider the ratio of the volume of the maximal pore at the crossover moment to the volume of the cylinder (sphere) without a void:

$$\Xi_{\text{cyl}} = \frac{(R_i^{\max})^2 - (R_{i0})^2}{(R_e^{\max})^2 - (R_i^{\max})^2}; \Xi_{sph} = \frac{(R_i^{\max})^3 - (R_{i0})^3}{(R_e^{\max})^3 - (R_i^{\max})^3}.$$

One can see from Fig. 5 that the pore formation in cylindrical samples is more efficient than that in spherical ones. As the initial radius of a particle increases, this efficiency tends to a certain asymptotic value. That is why, at large initial radii, the efficiency is determined by the chemical composition representing a moving force

Linear approximation coefficients of the dependences $R_i^{\max}(R_{e0})$ (Fig. 4) for cylinders at various average concentrations of the fast component $\bar{c}_B$

$\bar{c}_B$	$R_{e0}^{\max}/a$	$k(\bar{c}_B)$	$b(\bar{c}_B)$
0.025	15	0.12	0.27
0.075	10	0.22	0.12
0.100	6.75	0.26	0.09
0.200	4.5	0.36	–0.05
0.300	4.5	0.43	–0.14
0.400	3	0.48	–0.26
0.500	3	0.52	–0.45
0.600	4.5	0.56	–0.78
0.700	6.75	0.61	–1.70
0.800	15	0.67	–3.66

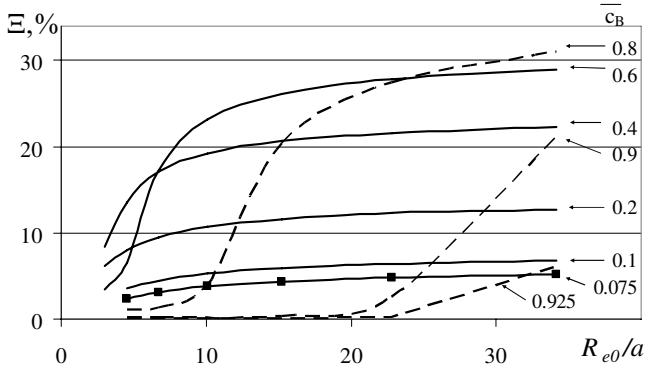

Fig. 6. Pore formation efficiency Ξ as a function of the initial radius of the particle R_{e0} for cylinders at various average concentrations $\bar{c}_B$

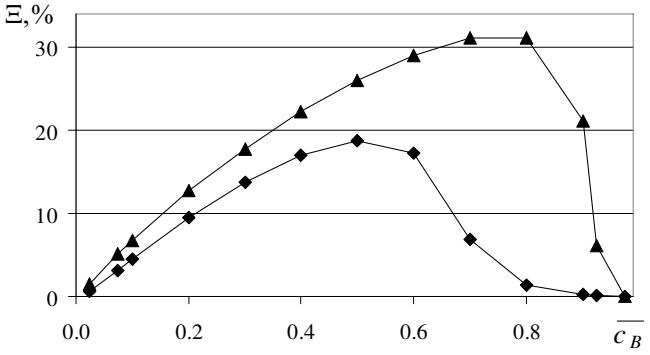

Fig. 7. Pore formation efficiency Ξ as a function of the average concentration $\bar{c}_B$ at various initial cylinder radii: small ($R_{e0} = 6.75a$, diamonds) and large ($R_{e0} = 34.2a$, triangles)

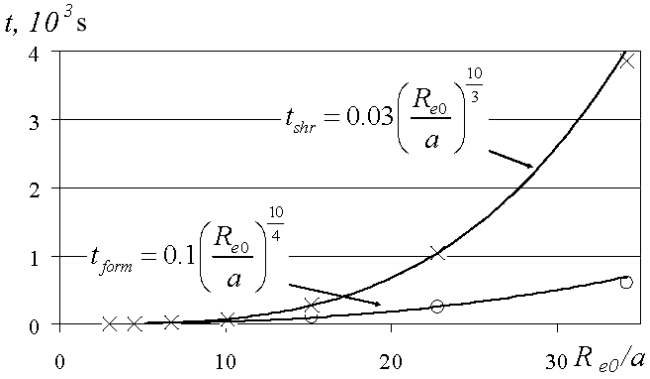

Fig. 8. Void formation time $t_{\rm form}$ (circles) and shrinking time $t_{\rm shr}$ (crosses) as functions of the initial radius of the particle R_{e0} for cylinders. $\bar{c}_B = 0.075$

of pore formation (Fig. 6). It is evident that the most efficient pore formation must be observed in the neighborhood of concentrations of 50 at.% with insignificant prevalence of the mobile component.

However, an increase of the cylinder radius results in a shift of the pore formation efficiency toward larger concentrations (0.7–0.8), Fig. 6. To our mind, this peculiarity is related to the radial symmetry of particles. For a particle with fixed outer radius R_{e0}, a rise of the concentration leads to the growth of the radius R_{BA} that determines the area of the reaction surface and, respectively, provides a higher pore formation efficiency.

The effect of the chemical composition on the pore formation efficiency can be traced by considering the dependences of Ξ on the average concentration of the fast component (Fig. 7): as the radius of a cylindrical particle increases, the efficiency grows with the gradual shift of the maximum toward higher concentrations. The asymmetry of $\Xi(\bar{c}_B)$ is related to the asymmetry of the diffusion core-shell pair and different mobilities of the components.

It is evident that the formation and the collapse of a larger void require more time. The formation time $t_{\rm form}$ and the shrinking time $t_{\rm shr}$ (introduced in Fig. 2) grow according to the power law with increase in the initial cylinder radius R_{e0} (Fig. 8). Moreover, a more rapid increase of the shrinking time as compared to the formation one (larger exponent) testifies to the fact that voids in cylinders of larger radii are more stable.

For the quantitative description of the stability of hollow shells (which is important for technological applications of nanotubes), let us analyze the ratio $t_{\rm shr}/t_{\rm total}$ of the absolute time of existence of a void before its collapse $t_{\rm shr}$ to the total lifetime $t_{\rm total} = t_{\rm form} + t_{\rm shr}$. If the stage of void formation is longer than that of its collapse, then $t_{\rm shr}/t_{\rm total} < 0.5$. In the opposite case, $t_{\rm shr}/t_{\rm total} > 0.5$. The closer the proposed ratio to 1, the more stable the pore.

One can see from Fig. 9 that, at small initial radii $R_{e0} = 3a \div 6.75a$, a pore collapses easier than it is formed ($t_{\rm form}/t_{\rm shr} < 0.5$). At large radii, the shrinking time is by an order of magnitude higher than the formation time ($t_{\rm form}/t_{\rm shr} \sim 0.9$). In this case, the maximum stability is reached at the average concentration $\bar{c}_B \sim 0.5$, in contrast to the maximum efficiency reached at $0.7 \div 0.8$. Such a non-coincidence at a significant concentration prevalence of the faster component can be due to its excess in the form of a thick interlayer in a vicinity of the inner surface at the crossover moment. In the case of a solid solution, this accelerates the collapse rather than impedes it.

In contrast to cylinders, the ratio $t_{\rm shr}/t_{\rm total}$ for spherically symmetric shells has a stronger dependence on the radius of an initial particle, which is explained by the different radius dependences of the volume (square for

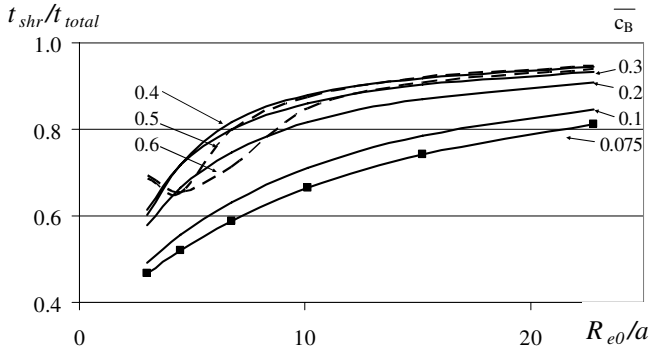

Fig. 9. Ratio $t_{\rm shr}/t_{\rm total}$ as a function of the initial cylinder radius R_{e0} at various concentrations $\overline{c}_B$

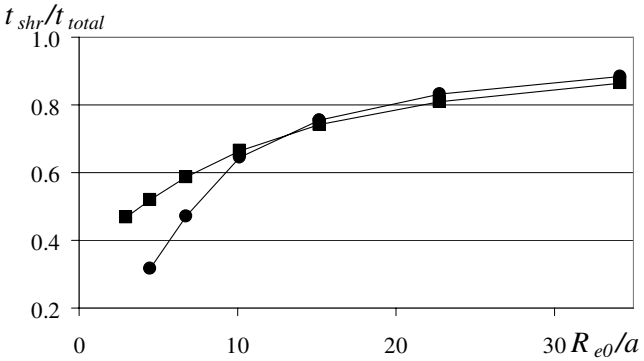

Fig. 10. Ratio $t_{\rm shr}/t_{\rm total}$ as a function of the initial cylinder radius R_{e0} for spheres (circles) and cylinders (squares). $\overline{c}_B = 0.075$

cylinders and cubic for spheres). As a result, spherical nanoshells very unstable at low radii (with the shrinking time twice larger than the formation one) reach the ratio $t_{\rm shr}/t_{\rm total} \sim 0.9$ with increase in the radius and even exceed the corresponding characteristic for cylindrically symmetric voids (Fig. 10). A rise of the concentration leads to a shift of the point, at which the stability of spheres starts exceeding that of cylinders, toward larger R_{e0}.

4. Conclusions

The phenomenological simulation allowed us to successively describe the stages of formation and collapse of a void in a cylindrical sample under constant external conditions. It was performed under the assumption that a void is formed along the cylinder axis and grows simultaneously over the whole length without partition into separate pores. The radius of the maximal cylindrical pore has a nearly linear dependence on the radius of the initial cylinder. The slope of such linear functions is proportional to the square root of the average concentration of the sample (in the interval $0 < \overline{c}_B \leq 0.8$).

The pore formation efficiency depends on the average concentration and radius of the initial particle: as the initial radius of the cylinder increases, the maximum efficiency is reached at a higher concentration of the fast component (a rise of the latter results in the growth of the radius $R_{BA} = \sqrt{\overline{c}_B} R_{e0}$ of the cylindrical interface of the core-shell system that determines the area of diffusion contact). In the case of a significant concentration prevalence of one of the components, the chemical moving forces get weaker, which, in turn, leads to the abrupt decrease of the pore formation efficiency. In cylindrical samples, this efficiency is larger than that in those with spherical symmetry.

The ratio of the void shrinking time in a nanoparticle to the total time of its existence is a function of the radius of the initial particle, average concentration, and shape: (1) the larger the particle radius, the more stable the shell); (2) the most stable are voids in samples with concentrations close to 50%; (3) at a specified concentration composition, there exists a critical initial radius: at lower radii, the stability of cylinder shells exceeds that of spherical ones and *vice versa*.

The work is performed under the support of the Ministry of Education and Science of Ukraine and the State Fund for Fundamental Researches of Ukraine.

The authors thank Prof. A.M. Gusak for fruitful consultations in the process of preparing this article.

1. F. Aldinger, Acta Metall. **22**, 923 (1974).
2. Ya.E. Geguzin, *Diffusion Zone*, (Nauka, Moscow, 1979) (in Russian).
3. Ya.E. Geguzin, Yu.I. Klinchuk, and L.N. Paritskaya, Fiz. Met. Metaloved. **43**, 602 (1977).
4. Y. Yin, R.M. Rioux, C.K. Erdonmez, S. Hughes, G.A. Somorjai, and A. P. Alivisatos, Science **30430,** 711 (2004).
5. Y. Yin, C.K. Erdonmez, A. Cabot, S. Hughes, and A.P. Alivisatos, Adv. Funct. Mater. **16**, 1389 (2006).
6. C.M. Wang, D.R. Baer, L.E. Thomas, J.E. Amonette, J. Antony, Y. Qiang, and G. Duscher, J. Appl. Phys. **98**, 094308 (2005).
7. R. Nakamura, D. Tokozakura, H. Nakajima, J.-G. Lee, and H. Mori, J. Appl. Phys. **101**, 074303 (2007).
8. D. Tokozakura, R. Nakamura, H. Nakajima, J.-G. Lee, and H. Mori, J. Mater. Res. **22**, 2930 (2007).
9. R. Nakamura, J.-G. Lee, D. Tokozakura, H. Mori, and H. Nakajima, Mater. Lett. **61**, 1060 (2007).
10. R. Nakamura, J.-G. Leez, H. Morix, and H. Nakajima, Philos. Mag. **88**, 257 (2008).

11. H.J. Fan, M. Knez, R. Scholz, D. Hesse, K. Nielsch, M. Zacharias, and U. Gösele, Nano Lett. **7**, 993 (2007).

12. R. Nakamura, G. Matsubayashi, H. Tsuchiya, S. Fujimoto, and H. Nakajima, Acta Mat. **57**, 4261 (2009).

13. T.C. Yih and M. Al-Fandi, J. Cell. Biochem. **97**, 1184 (2006).

14. K.N. Tu and U. Gösele, Appl. Phys. Lett. **86**, 093111 (2005).

15. A.M. Gusak, T.V. Zaporozhets, K.N. Tu, and U. Gösele, Philos. Mag. **85**, 4445 (2005).

16. R. Nakamura, D. Tokozakura, J-G. Lee, H. Mori, and H. Nakajima, Acta Mat. **56**, 5276 (2008).

17. A.M. Gusak and T.V. Zaporozhets, J. Phys.: Condens. Matter **21**, 415303 (2009).

18. G. Glodan, C. Cserhati, I. Beszeda, and D.L. Beke, Appl. Phys. Lett. **97**, 113109 (2010).

19. L. N. Paritskaya, Defect and Diffusion Forum **249**, 73 (2005).

20. A.M. Gusak and K.N. Tu, Acta Mat. **57**, 3367 (2009).

21. K.P. Gurov and A.M. Gusak, Metalofiz. **10**, 55 (1988).

22. A.V. Nazarov and K.P. Gurov, Fiz. Met. Metaloved. **37**, 496 (1973).

23. A.V. Evteev, E.V. Levchenko, I.V. Belova, and G.E. Murch, Diffusion Fundam. **6**, 19.1 (2007).

24. T.V. Zaporozhets, Visn. Cherkas. Univers. **141**, 103 (2008).

25. F. Hodaj and A.M. Gusak, Acta Mater. **52**, 4305 (2004).

26. J.W. Christian, *The Theory of Transformations in Metals and Alloys* (Pergamon Press, New York, 1975).

27. M.O. Pasichnyy, G. Schmitz, A.M. Gusak, and V. Vovk, Phys. Rev. **72**, 114 (2005).

Received 07.07.10.
Translated from Ukrainian by H.G. Kalyuzhna

ФОРМУВАННЯ І СТЯГУВАННЯ ПОРОЖНИН У НАНОДРОТАХ

О.М. Подолян, Т.В. Запорожець

Р е з ю м е

У межах феноменологічної моделі твердих розчинів описано двостадійний процес утворення порожнистих нанодротів у системі “ядро/оболонка” і їх стягування як результат конкуренції ефектів Френкеля, Гіббса–Томсона та оберненого ефекту Кіркендала. Досліджено залежності швидкості та ефективності процесу пороутворення від початкового радіуса циліндра та концентрації швидкого компонента. Дано порівняння з аналогічними результатами, отриманими для сферичносиметричних частинок.

Показано, що пороутворення ефективніше проходить у зразках циліндричної форми порівняно зі сферичною, а час існування порожнини залежить від радіуса нанооболонки.